JOURNAL OF NATURAL PRODUCTS

Article

pubs.acs.org/jnp

Isolation, Structure Elucidation, and Biosynthesis of an Unusual Hydroxamic Acid Ester-Containing Siderophore from *Actinosynnema mirum*

Tobias W. Giessen, Kamila B. Franke, Thomas A. Knappe, Femke I. Kraas, Mattia Bosello, Xiulan Xie, Uwe Linne, and Mohamed A. Marahiel*

Department of Chemistry/Biochemistry, Philipps-University, Hans-Meerwein-Strasse, D-35032 Marburg, Germany

Supporting Information

ABSTRACT: In this study we report the isolation, structure elucidation, and biosynthesis of mirubactin (**1**), a siderophore containing an unprecedented chemical functionality in natural products, namely, an *O*-acyl hydroxamic acid ester. Mirubactin represents the first siderophore isolated from the genus *Actinosynnema* and the first natural product produced by *Actinosynnema mirum* whose biosynthetic gene cluster could be identified. Structure elucidation was accomplished through a combination of spectroscopic (NMR, IR, and UV/vis) and mass spectrometric methods and revealed the presence of an unusual ester bond between the *δ*-*N*-hydroxyl group of *δ*-*N*-formyl-*δ*-*N*-hydroxyornithine and a 2,3-dihydroxybenzoate moiety. Bioinformatic analysis of the *A. mirum* genome and subsequent biochemical characterization of the putative biosynthetic machinery identified the gene cluster responsible for mirubactin assembly. The proposed biosynthesis of mirubactin comprises the iterative use of a stand-alone carrier-protein-bound substrate, as well as an ester-bond-forming step catalyzed by a C-terminal condensation domain, thus revealing an interesting system for further biochemical studies to gain a deeper understanding of nonribosomal peptide synthetase-catalyzed siderophore biosynthesis.

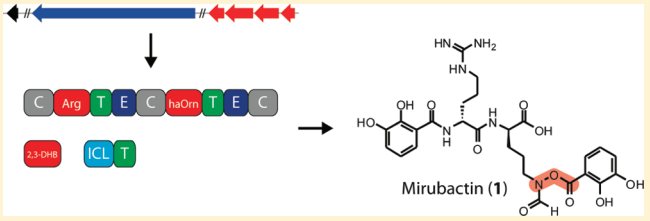

Most organisms require iron as an essential cofactor in a variety of metabolic processes associated with primary and secondary metabolism. In the presence of oxygen, soluble ferrous iron (Fe^{2+}) is spontaneously oxidized to its ferric form (Fe^{3+}), which, in aqueous environments at neutral pH, precipitates as insoluble ferric hydroxide complexes ($Fe(OH)_3$). The stability of these complexes leads to a very low bioavailability of ferric iron with concentrations of free Fe^{3+} ranging from 10^{-9} to 10^{-18} M in many microbial habitats, while pathogenic bacteria are faced with even lower concentrations in human serum.[1] This makes iron a key limiting factor of microbial survival in most aerobic environments as well as during the infection of host organisms through pathogenic microbes, causing selective pressure toward the development of specific iron acquisition mechanisms. One widely applied strategy by many microorganisms is the production and secretion of small-molecule iron-scavenging compounds termed siderophores, exhibiting very high affinities for ferric iron (K_f = 10^{22} to 10^{49} M^{-1}).[2] After extracellular iron binding and import of the ferric−siderophore complex by specific receptors, the iron is released and subsequently channeled to its intracellular targets.[3−5] The class of siderophores can be divided by their mode of assembly into nonribosomal peptide synthetase (NRPS)-dependent and NRPS-independent,[6] as well as by the moieties involved in iron coordination into catecholates, hydroxamates, carboxylates, and mixed forms thereof.[1,7]

In recent years, the increasing amount of whole genome sequencing data and ever more sophisticated bioinformatic tools have allowed the identification of formerly unknown/cryptic gene clusters and their assignment to the respective biosynthetic products. Nonribosomal peptide natural products are especially amenable to this approach due to the assembly line nature of their enzymatic machinery and the resulting collinearity between template and biosynthetic product often observed in these systems. Recently described siderophores where this approach was employed include coelichelin, fuscachelin A, rhodochelin, and amychelin.[8−11]

Species belonging to the genus *Actinosynnema*, which includes only two identified members so far, are known for their capability of producing biologically active compounds, as exemplified by the aldose reductase inhibitor thiazocin, the metalloprotease inhibitor propioxatin, the ansamitocin family of antitumor agents, and the nocardicins, belonging to the class of *β*-lactam antibiotics.[12−15] Whole genome sequencing of *Actinosynnema mirum* revealed that a significant part of its genome is dedicated to the production of secondary metabolites, indicating a vast potential for natural product biosynthesis.[16] So far, the only isolated natural products from *A. mirum* are the above-mentioned nocardicins (Figure 1A).[15] No secondary metabolite gene clusters in *A. mirum* could be identified and allocated to their biosynthetic products until now.

Received: January 9, 2012
Published: May 11, 2012

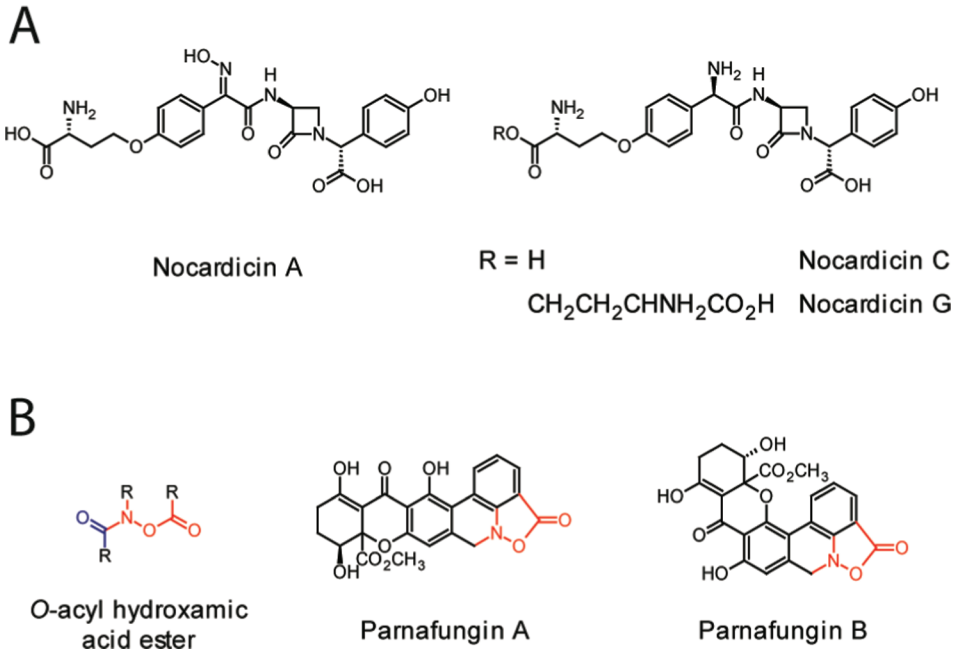

Figure 1. (A) Chemical structures of the nocardicin family of β-lactam antibiotics produced by *A. mirum*. (B) Structure comparison between an *O*-acyl hydroxamic acid ester and the cyclic *O*-acyl hydroxylamine moiety found in the parnafungin natural products isolated from *Fusarium larvarum*. The *N*-acyl group, differentiating a hydroxamic acid ester from the functionality found in the parnafungins, is highlighted in blue, while the connectivity found in both functional groups is shown in red.

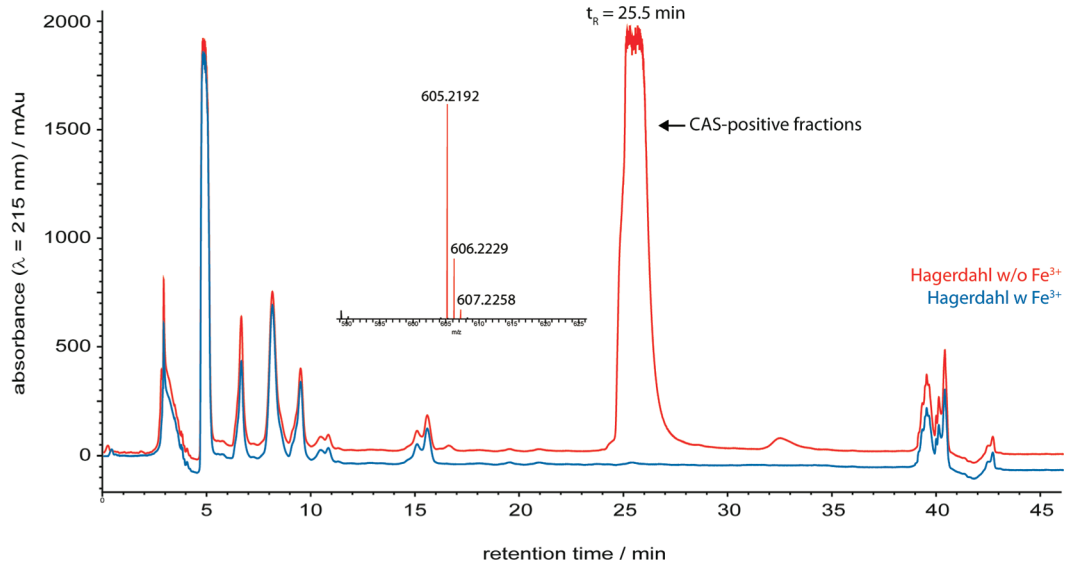

Figure 2. HPLC-MS traces of filtered culture supernatants. *A. mirum* was grown in Hagerdahl medium either in the absence (red) or in the presence (blue) of iron. A HRMS spectrum of the CAS-positive fractions is shown in the inset.

In this study we report the isolation, structure elucidation, and biosynthesis of mirubactin, the first siderophore isolated from the genus *Actinosynnema*, containing an unusual *O*-acyl hydroxamic acid ester group. Spectroscopic (NMR, UV/vis, and IR) and mass spectrometric (MS^n) studies established the presence of this functionality, which is to the best of our knowledge the first reported example of a naturally occurring *O*-acyl hydroxamic acid ester. The only natural products known so far containing a similar functionality are the parnafungins, which exhibit a cyclic *O*-acyl hydroxylamine moiety (isoxazolidinone), missing the additional *N*-acylation found in mirubactin (Figure 1B).[17] Through bioinformatic analysis of the *A. mirum* genome and subsequent biochemical characterization of the proposed biosynthetic machinery we were able to confidently identify the biosynthetic gene cluster responsible for mirubactin assembly.

RESULTS AND DISCUSSION

Isolation and Structure Elucidation of Mirubactin (1). The production of siderophores as a response to iron-limited conditions is tightly regulated. To force their production in a laboratory experiment, we cultivated *A. mirum* in iron-depleted Hagerdahl medium at 28 °C. The production of iron-scavenging compounds was monitored via the chrome azurol S (CAS) liquid assay performed directly with culture supernatant.[18] The first CAS-positive reaction could be

dx.doi.org/10.1021/np300046k | J. Nat. Prod. 2012, 75, 905−914

observed 3 days after inoculation. Subsequently samples were prepared for preparative HPLC analysis by centrifugation and filtration of the supernatant. Application of an extraction protocol was dismissed after realizing that MeOH, *n*-butanol, or XAD-16 resin extractions yielded preparative HPLC samples of lesser purity than a simple filtration and direct use of the culture supernatant. Fractionation by preparative HPLC was monitored by the absorptions at 215 and 280 nm as well as by checking the resulting fractions for CAS activity. In comparison with the iron-containing control only one additional CAS-positive peak could be observed, with a retention time of 25.5 min (Figure 2). HRMS analysis of the respective fractions confirmed the presence of one main compound, with a m/z of 605.2192 ($[M + H]^+$), corresponding to the chemical formula $C_{26}H_{33}N_6O_{11}^+$. The discovered iron-scavenging compound, which will subsequently be referred to as mirubactin (**1**), could be obtained in an overall yield of 286 mg/L culture. Following large-scale purification mirubactin was subjected to MS^n analysis in order to acquire some initial information about its individual building blocks and their connectivity. MS^2 as well as MS^3 fragmentation was carried out by performing collision-induced dissociation (CID) experiments. MS^2 fragmentation yielded a major fragment ion with a m/z of 469.2040 ($[M + H]^+$, calculated m/z 469.2042), which could be associated with the tripeptide ion of 2,3-DHB-Arg-fhOrn (2,3-DHB = 2,3-dihydroxybenzoate; fhOrn = *δ-N*-formyl-*δ-N*-hydroxyornithine), resulting from a neutral loss of dehydrated 2,3-DHB (dh-2,3-DHB, observed m/z 136.0160, calculated m/z 136.0160), in accordance with the fact that *ortho*-hydroxylated benzoic acid derivatives are known to form benzodioxetanes during MS^n gas-phase fragmentation.[19]

Additional fragment ions observed correspond to the consecutive loss of two dh-2,3-DHB moieties (observed m/z 333.1886, calculated m/z 333.1881) and the loss of dh-2,3-DHB along with fhOrn (observed m/z 293.1248, calculated m/z 293.1244), giving rise to the dipeptide ions Arg-fhOrn and 2,3-DHB-Arg, respectively (Figure 3 and Supporting Information, Figure S1). To gain further information about the respective constituents, the main fragment resulting from MS^2 fragmentation was subjected to MS^3 analysis. The MS^3 spectrum showed two main signals, one belonging to the already mentioned ion with m/z 333.1886, originating from a second loss of dh-2,3-DHB from the 2,3-DHB-Arg-fhOrn tripeptide fragment, while the second one (observed m/z 311.1350, calculated m/z 311.1350) can be assigned to a 2,3-DHB-Arg dipeptide fragment (Figure 3B and Supporting Information, Figure S2). Additionally two low-abundance ions were observed exactly matching the calculated masses of Arg (observed m/z 175.1190, calculated m/z 175.1190) and fhOrn (observed m/z 177.0870, calculated m/z 177.0870). In summary, the MS^n analysis revealed that mirubactin consists of two 2,3-DHB building blocks, one arginine and one fhOrn. The observed fragmentation pattern can be explained only by a tetrapeptide with the following N- to C-terminal connectivity: 2,3-DHB-Arg-fhOrn-2,3-DHB. How the C-terminal 2,3-DHB is connected to the fhOrn moiety cannot be deduced from the MS^n studies alone.

Building on the structural information obtained through MS^n fragmentation, the final structure of mirubactin was determined using NMR spectroscopy. On the basis of the chemical shift values and the coupling patterns of the observed signals in the ^1H spectrum, one arginine, one *δ-N*-formyl-*δ-N*-hydroxyornithine (fhOrn), and two 2,3-DHB building blocks were

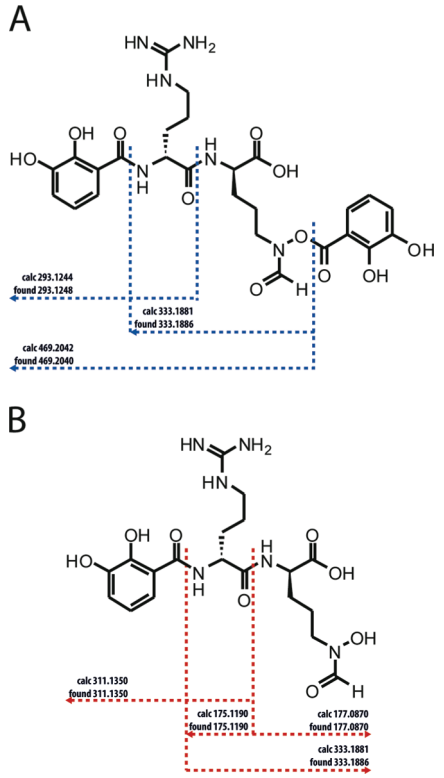

Figure 3. Main fragments observed during MS^2 (A) and MS^3 (B) CID fragmentation experiments.

identified (Supporting Information, Table S1). The connectivity among these moieties and the final structure of mirubactin (Figure 4) were determined by using the information obtained through two-dimensional NMR spectra. The ^1H spectrum

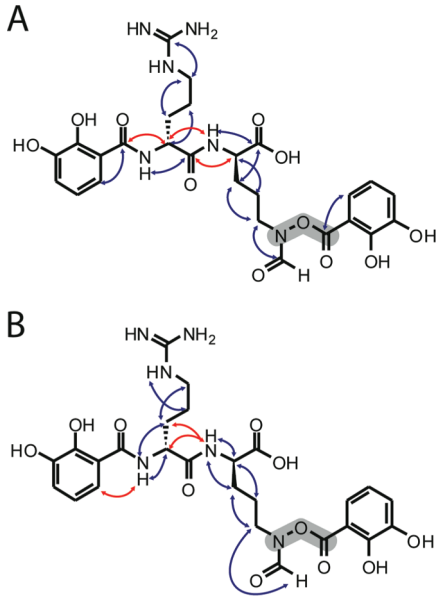

Figure 4. Structure of **1** as determined by NMR. The connectivity shown is DHB[1]-Arg-fhOrn-DHB[2]. The fhOrn *δ-N* acylation is highlighted in gray. (A) Long-range $^1H-^{13}C$ correlations observed in DMSO-d_6 at 300 K (blue: intraresidue contacts, red: long-range inter-residue contacts). (B) NOE contacts observed in DMSO-d_6 at 300 K (blue: intraresidue contacts, red: long-range inter-residue contacts).

dx.doi.org/10.1021/np300046k | *J. Nat. Prod.* 2012, 75, 905−914

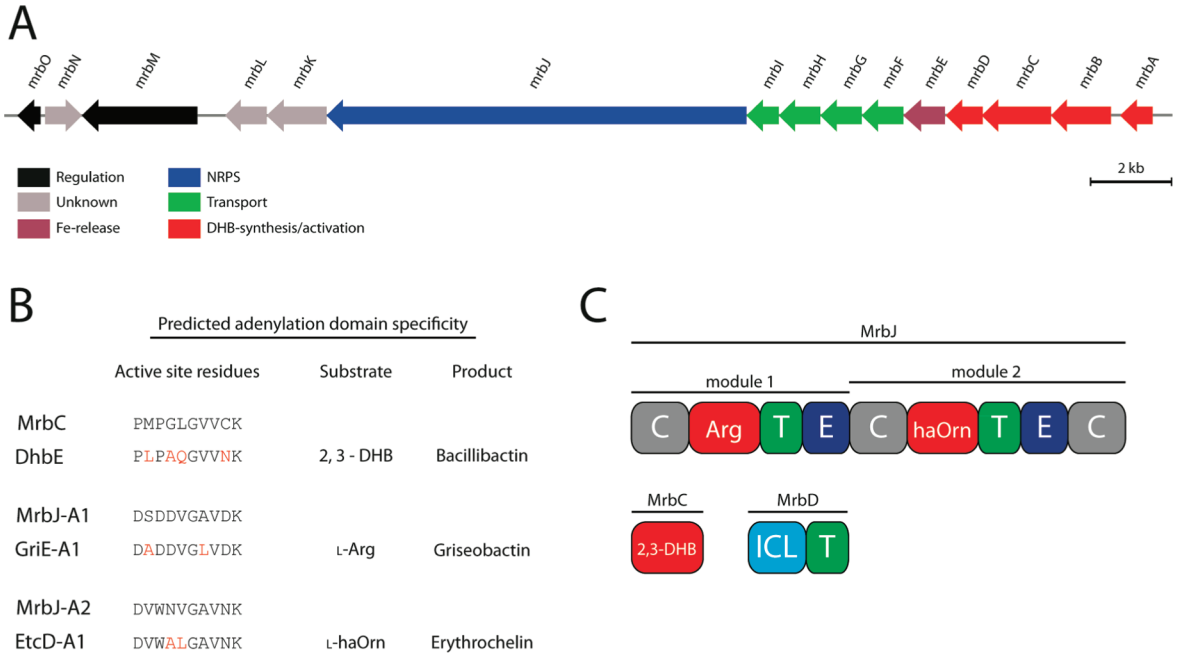

Figure 5. Bioinformatic overview of the mirubactin biosynthetic gene cluster. (A) *mrb*-Gene cluster responsible for mirubactin assembly. (B) Comparison of the predicted A-domain specificities of MrbJ-A1/A2 and MrbC with characterized A-domains of known NRPS products. Differences are highlighted in red. (C) Gene products of MrbJ, MrbC, and MrbD directly involved in mirubactin assembly, showing the respective NRPS domain organization.

revealed the presence of two amide protons, at 8.80 and 8.37 ppm. Two cross-peaks verifying the presence of two amino acids were observed in the $^{1}H-^{15}N$ HSQC spectrum. TOCSY cross-peaks confirmed the presence of one arginine and one ornithine. NOE contacts between H-6 of DHB[1] and the NH of Arg as well as between H-α of Arg and the NH of fhOrn were observed, which served as evidence for the sequential connections DHB[1]–Arg and Arg–fhOrn, respectively. Long-range $^{1}H-^{13}C$ correlations identified the amide connections along DHB[1], Arg, and fhOrn (Supporting Information, Figures S3, S4, S5). The $^{1}H-^{15}N$ HSQC spectrum revealed amide nitrogen chemical shifts of 118.2 and 118.3 ppm for Arg and Orn, while the long-range $^{1}H-^{15}N$ HMBC spectrum showed signals at 177.3 and 178.4 ppm for the N-6 of Orn. These latter ^{15}N chemical shifts reflect the presence of a tertiary nitrogen (N-6) and the formation of an N–O bond at N-6 (Supporting Information, Figure S6). Two sets of signals of comparable intensity were observed for the side chain and the α-substituent of fhOrn. Similar sets of signals were observed in rhodochelin and the Ga^{3+}-erythrochelin complex, as well as in pyoverdin.[9,20,21] This observation can be explained by the existence of a cis–trans isomerism along the C–N bond of the formyl group, resulting from its partial double-bond character. The almost 1:1 (*Z*:*E*) ratio of these signals, in contrast to the usually observed 3:1 (*Z*:*E*) ratio,[21] indicates that no free δ-*N*-hydroxyl group is present. Instead a sterically demanding residue is bound via this group, resulting in two energetically equivalent isomers, which is reflected in the signal ratio mentioned above. The assigned ^{1}H, ^{13}C, and ^{15}N chemical shifts are listed in the Supporting Information, Table S1. The observed NOE contacts and the long-range $^{1}H-^{13}C$ correlations are shown in Figure 4A and B, respectively.

Additional IR and UV/vis spectroscopic analyses were able to confirm the mirubactin structure initially determined by MS^{n} and NMR. IR spectroscopy clearly showed the presence of an oxo-ester, thus directly confirming the unusual connectivity observed in the fhOrn side chain, resulting in an *O*-acyl hydroxamic acid ester functionality (Supporting Information, Figure S6). UV/vis spectroscopic analysis of *holo*-mirubactin (**2**) indicates that only catecholate coordinating groups are present in the ferric–siderophore complex, implied by the broad absorption band at 510 nm characteristic of a catecholate ligand–metal charge transfer (LMCT).[22] On the other hand, no LMCT typical for hydroxamate coordinating groups in siderophores (about 440 nm) could be observed (Supporting Information, Figure S8).[23] These results indicate that no free hydroxamate moiety is involved in iron binding, which is in accordance with the mirubactin structure.

Amino acid stereoconfiguration was determined by applying Marfey's method,[24] where the constituents of a mirubactin acid hydrolysate were derivatized using FDAA. The resulting reaction mixture was subjected to HPLC-MS analysis. Comparison with synthetic amino acid standards revealed that D-Arg and D-fhOrn are present in mirubactin (Supporting Information, Figure S9).

Taking all this information into account, we were able to establish the structure of the newly discovered siderophore mirubactin. It consists of a D-Arg-D-fhOrn core, carrying both a N- and C-terminal 2,3-DHB moiety. The N-terminal 2,3-DHB is bound to the α-amino group of D-Arg via a standard peptide bond, while the 2,3-DHB located at the C-terminus is attached to the δ-*N*-hydroxyl group of the D-fhOrn moiety, forming an *O*-acyl-hydroxamic acid ester. This unusual connectivity leads to the curious phenomenon that one functionality capable of coordinating iron (hydroxamate) is masked by a different type of coordinating group (catecholate). A possible rationalization for this occurrence is that catecholates are known to bind iron more tightly than hydroxamates. The reason for the superior affinity of catecholates to ferric iron stems from the fact that they incorporate two hard oxygen donor atoms to form a five-

dx.doi.org/10.1021/np300046k | *J. Nat. Prod.* 2012, 75, 905–914

membered chelate ring, with electron density delocalized around the phenyl ring.[25] This and the fact that no other reasonable option for catecholate attachment is present in the molecular scaffold at hand could explain this unusual structure. This would lead to a siderophore with increased binding affinity, improving the organism's capability to thrive under iron-limited conditions and thereby conveying an evolutionary advantage. A second possible explanation for the unusual building block connectivity found in mirubactin is that decreasing the number of different coordinating groups in a siderophore could be advantageous due to the fact that siderophore uptake systems usually employ receptors capable of recognizing only certain types of ferric−siderophore complexes based on the coordinating groups present. This would lead to a situation where less competitive organisms would be able to hijack the iron-loaded siderophore in question.[26,27]

Bioinformatic Analysis of the *A. mirum* Genome and Identification of a Putative Mirubactin Gene Cluster. Today the availability of whole genome sequencing data often allows the identification and subsequent activation of cryptic biosynthetic gene clusters through genome mining and modulation of transcription factor expression levels, which has proven to be a successful approach toward the identification of novel secondary metabolites.[28,29] On the other hand, genome data permit the bioinformatic search for putative secondary metabolite gene clusters and their assignment to known or newly discovered natural products.[29]

The *A. mirum* genome sequence was published at the end of 2009, but so far it was not possible to experimentally connect a gene cluster with the production of a specific secondary metabolite.[16]

To establish a connection between mirubactin and its biosynthetic genes, the genome of *A. mirum* was thoroughly analyzed for putative siderophore gene clusters. Two gene clusters putatively responsible for siderophore assembly and transport could be identified. The first one exhibits characteristics of a hydroxamate-type siderophore gene cluster[30] (Supporting Information, Figure S10), while the second one resembles gene clusters involved in mixed catecholate−hydroxamate biosynthesis (Figure 5A).[10] Due to the observed domain organization as well as A-domain substrate predictions, the first cluster could be excluded as the mirubactin biosynthetic gene cluster. Instead we propose that it is responsible for the biosynthesis of a foroxymithine/erythrochelin-like cryptic siderophore, based on the high sequence homology of *Amir_5064* to EtcD (61% identity, 72% similarity), the NRPS responsible for erythrochelin biosynthesis in *Saccharopolyspora erythraea*,[20,30] and the matching modular organization as well as A-domain substrate predictions (Supporting Information, Figure S10). Additionally high homology is found to *RHA1_ro04715* from *Rhodococcus jostii* RHA1, proposed to be involved in the assembly of a foroxymithine derivative, and to a putative foroxymithine gene cluster recently identified in *Streptomyces pristinaespiralis* employing a PrISM-based method (proteomic investigation of secondary metabolism).[9,31,32] Despite the presence of the gene cluster discussed above, no foroxymithine-like siderophore could be isolated from *A. mirum* cultures under iron-starvation conditions. The second identified siderophore cluster covers approximately 29 kbp and contains 15 open reading frames (ORFs). On the basis of the following remarks we propose that this gene cluster is responsible for mirubactin assembly; consequently the genes from *Amir_2714* to *Amir_2728* have been renamed as *mrbA* to *mrbO*. The largest gene in the cluster (9.9 kbp), designated *mrbJ*, encodes a nonribosomal peptide synthetase consisting of two modules. In addition to the canonical elongation domains (C: condensation, A: adenylation, T: thiolation) both modules contain an epimerization (E) domain located between the upstream T- and the downstream C-domains, indicating the presence of D-configured building blocks in the assembly line product. These findings are in accordance with the experimentally determined α-C stereoconfigurations of the mirubactin constituents discussed in the previous section (Figures 3 and 4, Supporting Information, Figure S9). Interestingly, the second module contains no carboxy-terminal thioesterase domain usually found in bacterial NRPS termination modules,[33] but a C-terminal condensation domain. Condensation domains located at the C-terminus of termination modules have been proposed to catalyze intramolecular cyclization by ester bond formation in rapamycin[34] and FK506[35] biosynthesis, thus releasing the product from the assembly line. Condensation domains in NRPS termination modules are also widely used in fungal NRPS systems often catalyzing ester bond formation.[36,37] These findings indicate that the C-terminal condensation domain of MrbJ could be responsible for the formation of the hydroxamic acid ester found in mirubactin (Figures 3 and 4). Substrate specificity prediction of the two adenylation domains found in MrbJ proposes a preference for L-Arg and L-haOrn (δ-*N*-acetyl-δ-*N*-hydroxy-L-ornithine), respectively (Figure 5B).[30,38] These predictions are in accordance with the presence of Arg and fhOrn building blocks in the mirubactin structure, solved by NMR and MS^n. In addition the biochemical characterization of the MrbJ-associated A-domains confirms the bioinformatic predictions, which will be discussed in more detail in the following section.

The ORFs *mrbA* to *mrbD* located upstream of *mrbJ* share sequence homology to characterized genes responsible for 2,3-DHB biosynthesis starting with the precursor chorismate.[39,40] *mrbA* to *mrbC* are annotated as 2,3-dihydro-DHB dehydrogenase, isochorismate synthase, and DHB-AMP-ligase, respectively. Bioinformatic substrate specificity prediction[41] indicates that *mrbC* is indeed a 2,3-DHB-specific stand-alone adenylation domain and thus putatively responsible for the activation of the two 2,3-DHB moieties found in mirubactin (Figures 3 and 4).[42] After activation MrbC likely tethers the respective 2,3-DHB monomer to a dedicated carrier protein. The gene product of *mrbD* shares sequence homology with a bifunctional enzyme containing a N-terminal isochorismate lyase domain and a C-terminal carrier-protein domain (DhbB) found in 2,3-DHB biosynthesis and is thus presumably the interaction partner of MrbC.[43] A biochemical characterization of MrbC confirms its predicted role in mirubactin biosynthesis, as shown in the following section.

The genes *mrbF* to *mrbI* correspond to a siderophore transport system, with *mrbF* being annotated as a substrate-binding protein, *mrbG* and *mrbH* as permeases, and *mrbI* as an ATPase. They putatively form an ABC-type transport system where the transmembrane domain consists of a heterodimeric complex of MrbG and MrbH and the nucleotide-binding domain comprises of an MrbI homodimer. The gene product of *mrbF* shows the typical N-terminal signal peptide sequence and cysteine residue for covalent lipid-anchor attachment usually found in substrate-binding proteins of Gram-positive bacteria.[44] MrbF could be shown to selectively bind *holo*-mirubactin (**2**),

confirming its role as a substrate-binding protein (data not shown).

An additional ORF located in the proposed mirubactin gene cluster, designated *mrbE*, shows homology to the ferric siderophore reductases YqjH and ViuB from *E. coli* and *V. cholerae*, respectively.[45,46] Thus a role in intramolecular iron release from ferric−mirubactin is proposed for MrbE.

The absence of genes responsible for ornithine modification in the proposed mirubactin gene cluster led to a genome-wide search for putative candidate enzymes. By using the characterized FAD-dependent monooxygenase EtcB from the erythrochelin system[47] as a query, we were able to identify *Amir_5066* (64% identity, 76% similarity), annotated as an L-ornithine-5-monooxygenase, located in the putative foroxymithine/erythrochelin gene cluster discussed above. Being the only hit with significant homology to EtcB, it is likely that *Amir_5066* is involved in L-Orn modification for subsequent use in mirubactin biosynthesis (Figure 7). Continuing the search for the second L-ornithine-modifying enzyme responsible for the *δ-N*-formylation of the ornithine moiety found in mirubactin, we identified *Amir_1095*, which is annotated as a formyltransferase domain, by using the *δ-N*-L-ornithine formyltransferase *RHA1_ro04712* from the rhodochelin system as a query.[9,48] The high sequence homology shared between these enzymes (63% identity, 80% similarity) and the fact that *Amir_1095* is the only formyltransferase besides the Met-tRNA formyltransferase (*Amir_5224*) encoded in the *A. mirum* genome led us to propose the involvement of *Amir_1095* in L-ornithine modification. Interestingly *Amir_1095* shares sequence homology with the N-terminal domain of ArnA (31% identity, 49% similarity), a bifunctional enzyme involved in polymyxin resistance, where the formyltransferase domain catalyzes the *N*-formylation of UDP-L-Ara4N, yielding UDP-*β*-L-Ara4FN, and the C-terminal domain catalyzes the decarboxylation of UDP-glucuronic acid.[49] Similar systems where precursor-modifying enzymes are dispersed throughout the genome and not encoded in the biosynthetic locus featuring the NRPS assembly line have been reported for the siderophores erythrochelin from *S. erythraea* and rhodochelin from *R. jostii* RHA1.[9,47]

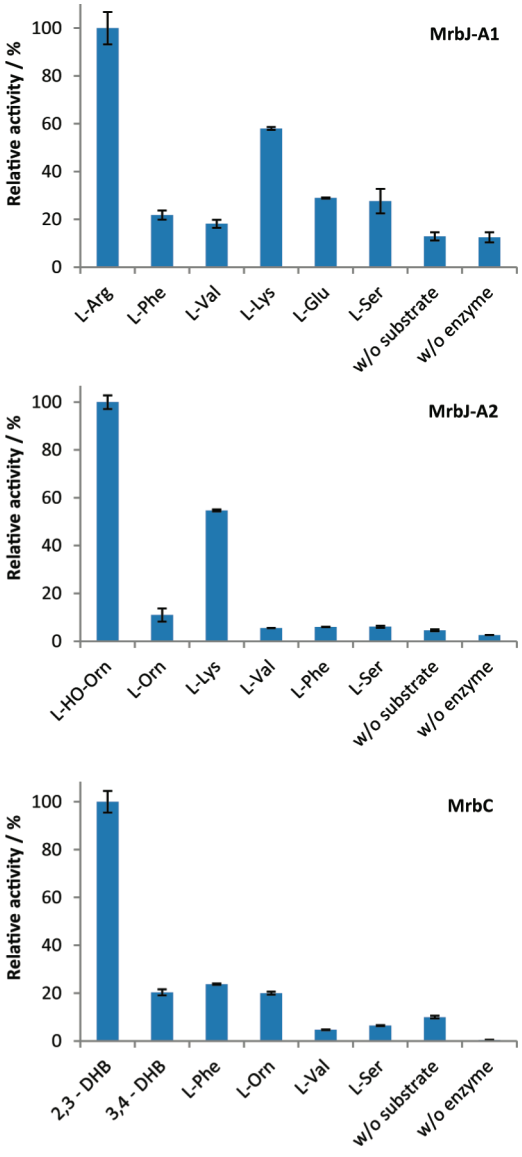

Figure 6. Biochemical characterization of MrbJ-A1/A2 and MrbC, using the pyrophosphate exchange assay. Shown are the respective relative activities of various (amino) acids.

Using the online resource antiSMASH,[50] capable of identifying biosynthetic loci in whole genome sequences and comparing them to databases, thereby allowing similar gene clusters in different organisms to be found and compared, we were able to discover gene clusters in *Streptomyces* sp. ACTE and *Saccharomonospora viridis*, closely resembling the proposed mirubactin gene cluster (Supporting Information, Figure S11). It is therefore likely that these organisms are capable of producing mirubactin-like siderophores when facing iron-limited conditions.

A complete bioinformatic overview of the *mrb*-gene cluster is presented in the Supporting Information, Table S2.

Characterization of Mirubactin Biosynthetic Genes and Proposed Biosynthesis. To provide experimental evidence that the *mrb*-gene cluster is indeed responsible for the *in vivo* production of mirubactin in *A. mirum*, all three adenylation domains predicted to be involved in mirubactin assembly were characterized in vitro employing the well-established pyrophosphate exchange assay. The two A-domains found in MrbJ were excised using the procedure detailed in the Experimental Section and, together with the stand-alone A-domain MrbC, cloned into *E. coli* expression vectors. Subsequent overexpression and purification by affinity chromatography yielded the three proteins as C-terminal His_6-fusions (Supporting Information, Figure S12). The respective bioinformatically predicted monomers were assayed along with selected substrates representing different amino acid classes based on their chemical properties. In the case of MrbC, the structurally related 3,4-DHB was additionally tested for activation. In the MrbJ-A2 assay, hOrn (hydroxy-L-ornithine), chemically synthesized by an established protocol,[51] was used instead of the expected fhOrn due to the fact that no protocol for fhOrn synthesis is present in the literature. The results presented in Figure 6 show a significant preference for the predicted monomers in all three cases. MrbJ-A1 shows the highest activity for L-Arg, while the second strongest activation is observed for L-Lys. Background levels are quite high in the MrbJ-A1 assay, indicating a moderate overall adenylation activity of the first MrbJ A-domain. Turning to MrbJ-A2 the results clearly show a preference for L-hOrn. Interestingly the second highest signal is observed for L-Lys, explainable by the

dx.doi.org/10.1021/np300046k | J. Nat. Prod. 2012, 75, 905−914

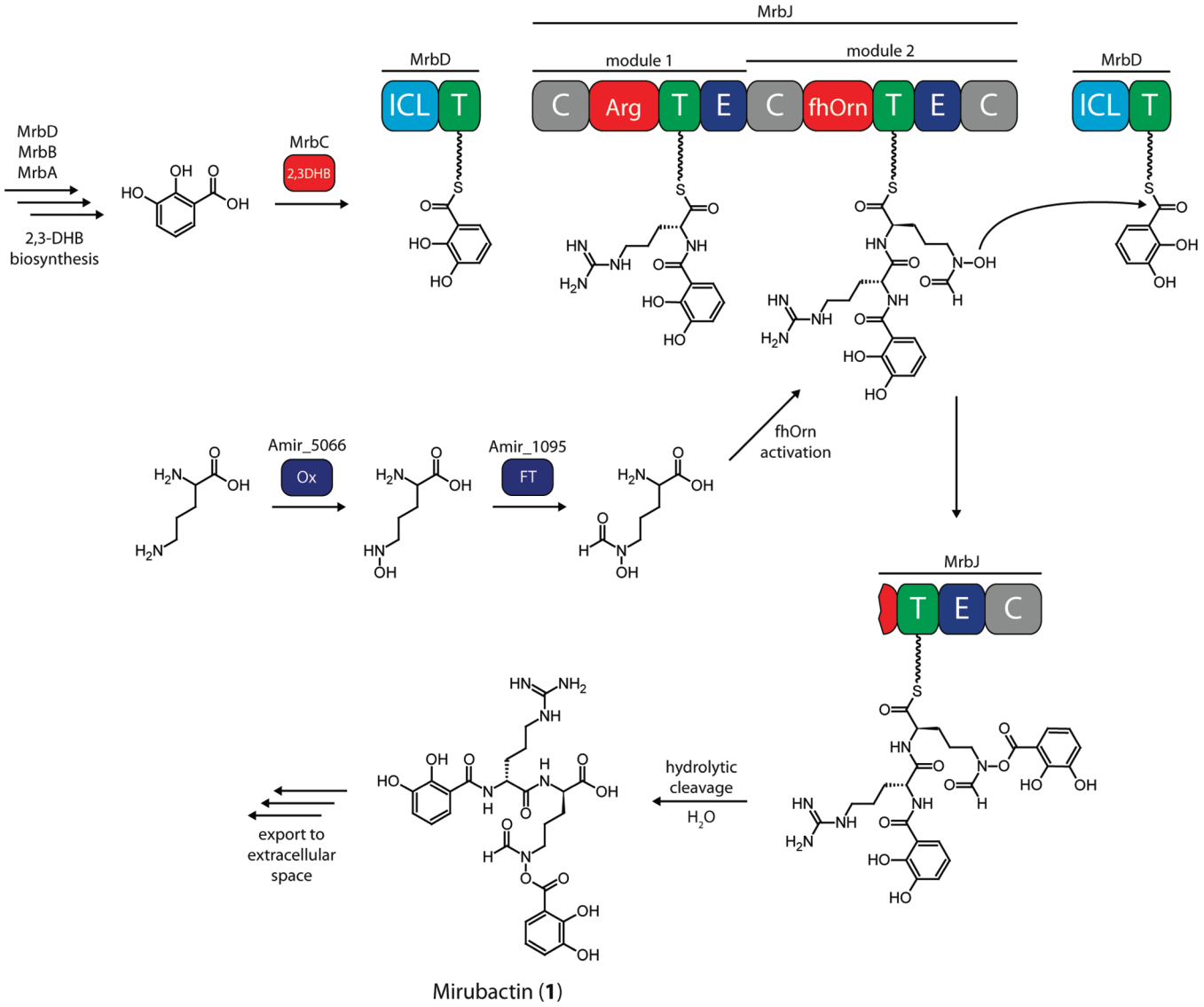

Figure 7. Proposed biosynthetic pathway for mirubactin assembly. Before assembly of the tripeptide by the NRPS MrbJ, the two nonproteinogenic building blocks 2,3-DHB and fhOrn are synthesized by the corresponding pathways as indicated. Attachment of the second 2,3-DHB moiety through the attack of the *δ*-*N*-hydroxyl in the fhOrn side chain is followed by a hydrolytic cleavage of the tetrapeptide and its export to the extracellular space. ICL: isochorismate lyase, Ox: oxidoreductase, FT: formyltransferase.

fact that it has the same side-chain length as L-hOrn, while L-Orn shows a signal only slightly over background level. This phenomenon was previously observed in the L-hOrn activating termination module in the fuscachelin system from *Thermobifida fusca*.[10]

The results obtained for the stand-alone adenylation domain MrbC again support the bioinformatic prediction by showing a clear preference for 2,3-DHB, while the structurally related 3,4-DHB and the other tested substrates show only background level intensities.

Taken together, these results establish the role of the NRPS MrbJ in the mirubactin biosynthetic pathway and demonstrate that the proposed biosynthetic gene cluster inferred from bioinformatic analysis and reasoning is indeed responsible for mirubactin biosynthesis in *A. mirum*. Additionally the preferred activation of L-hOrn by MrbJ-A2 indicates that L-Orn side-chain hydroxylation takes place before activation by and tethering to the MrbJ assembly line. We are unaware of any studies on L-fhOrn precursor biosynthesis in the literature, but a recent investigation of a similar system in *S. erythraea* showed that hydroxylation of L-Orn is the first step in L-haOrn generation, followed by acetylation of free L-hOrn, firmly establishing that both modifying enzymes act on the free precursor before tethering to the NRPS assembly line.[47] This led us to propose that L-fhOrn is generated by the action of the two above-mentioned tailoring enzymes (*Amir_5066* and *Amir_1095*) followed by its activation and further processing by the NRPS MrbJ, keeping in mind that we cannot exclude that formylation takes place on a carrier-protein-tethered substrate.

The predicted biosynthesis of mirubactin (Figure 7) contains several unusual features that will be elaborated on in the following paragraph. Mirubactin assembly is initiated by the activation of a 2,3-DHB molecule through MrbC and its subsequent tethering to its cognate carrier protein, which is part of the bifunctional enzyme MrbD. After assembly of the tripeptide DHB-D-Arg-D-fhOrn through the action of MrbJ, where the activated L-Arg and L-fhOrn monomers are epimerized by the respective E-domains embedded in both

dx.doi.org/10.1021/np300046k | *J. Nat. Prod.* 2012, 75, 905−914

NRPS modules, the resulting intermediate is bound via a thioester linkage to the T-domain of the second module. Now a second activated 2,3-DHB moiety, again bound to MrbD, is attacked by the δ-*N*-hydroxyl group in the ornithine side chain, representing the only viable nucleophile, thus establishing the unusual *O*-acyl hydroxamic acid ester linkage. We propose that this step is more likely to occur while the intermediate is still bound to the NRPS machinery due to a favorable spatial positioning of the attacking nucleophile and the respective electrophile putatively facilitated by protein−protein interactions between MrbJ and MrbD. This strategy is often used in the NRPS system to carry out regiospecific transformations on T-bound peptidyl substrates, for example in the case of trans-acting tailoring enzymes.[52] If the tripeptide was hydrolyzed before attachement of the second 2,3-DHB moiety, a nucleophilic attack would be less likely to occur due to diffusion of the now soluble tripeptide molecule. A subsequent hydrolytic cleavage of the tetrapeptide DHB-D-Arg-D-fhOrn-DHB results in the mature mirubactin siderophore, which can now be exported to the extracellular space to fulfill its biological function as an iron scavenger. It is likely that hydroxamic acid ester bond formation is catalyzed by the C-terminal condensation domain of MrbJ. Further examples of ester bond formation by NRPS condensation domains can be found in the biosynthesis of the antitumor antibiotic C-1027, where the stand-alone C-domain SgcC5 forms an oxo-ester between a T-bound substrate and a soluble nucleophile, as well as in fumonisin biosynthesis, where the C-terminal condensation domain of Fum14 catalyzes a similar transformation, also resulting in an oxo-ester.[53,54] Additionally, ester bond formation is proposed to be catalyzed by the two already mentioned C-terminal condensation domains in the rapamycin and FK506 systems, respectively.[34,35]

In conclusion mirubactin is the first siderophore isolated from the genus *Actinosynnema*, featuring to the best of our knowledge an unprecedented chemical functionality in natural products, namely, an *O*-acyl hydroxamic acid ester. Why the second coordinating catecholate group is installed on the side-chain hydroxamate of the C-terminal ornithine moiety, thus masking a coordinating group already in place, has to be the subject of further investigation. Additionally the iterative use of carrier-protein-bound 2,3-DHB and the ester-bond-forming step itself make mirubactin biosynthesis a highly interesting system for further biochemical investigations to gain a deeper understanding of NRPS-catalyzed siderophore biosynthesis.

EXPERIMENTAL SECTION

General Experimental Procedures. UV−vis spectra were recorded on an Ultrospec 3000 (Pharmacia) spectrophotometer. Wavescan measurements were performed in a wavelength range from 300 to 700 nm and a scan rate of 750 nm/min. To record the UV−vis absorption spectra of *holo*-mirubactin (**2**), a 100 μM solution in water was used. The *holo*-complex was generated by incubating mirubactin with an equimolar amount of aqueous $FeCl_3$ for 10 min at room temperature prior to performing the measurements. For IR measurements a KBr disk of purified mirubactin (**1**) was prepared and subjected to FT-IR spectroscopic analysis on a Magna-IR 750 spectrometer (Nicolet). For NMR studies 8 mg of the title compound was dissolved in 280 μL of DMSO-d_6. Two-dimensional experiments were performed on a Bruker AV600 spectrometer with a TXI $^1H-^{13}C/^{15}N$ probe installed with *z* gradient. For ^{13}C experiments about 12 mg of the compound was dissolved in 100 μL of DMSO-d_6 in a 3 mm Shigemi tube matched to DMSO. ^{13}C spectra were recorded on a Bruker AV500 spectrometer with a BBFO probe. The one-dimensional ^1H and ^{13}C spectra, the homonuclear two-dimensional DQF-COSY, TOCSY, NOESY, and ROESY spectra, the $^1H-^{13}C$ HSQC and HMBC spectra, and the $^1H-^{15}N$ HSQC and $^1H-^{15}N$ HMBC spectra were recorded with standard pulse programs at room temperature.[55] The TOCSY spectrum was recorded with a mixing time of 80 ms, whereas NOESY and ROESY spectra were taken at 150 and 300 ms mixing times. The 1D spectra were acquired with 65 536 data points, whereas the 2D spectra were collected using 4096 points in the F_2 dimension and 512 increments in the F_1 dimension. For 2D spectra 32−64 transients were used, while the ^{13}C spectrum was recorded with 32 K scans. The relaxation delay was 2.5 s. For the $^1H-^{15}N$ HMBC experiment 19 mg of mirubactin was dissolved in 120 μL of DMSO-d_6 in a 3 mm Shigemi tube matched to DMSO. The experiment was optimized for a long-range coupling constant of 2 Hz. The spectrum was recorded with 128 transients in the F_2 dimension, and the typical experiment time was about 2 days. The ^1H and ^{13}C chemical shifts were referenced to solvent signals. The spectra were processed using Bruker Topspin 2.1. MS fragmentation experiments were carried out on a LTQ-FT instrument (Thermo Fisher Scientific) by collision-induced dissociation fragmentation using an online syringe pump for injection. RP-LCMS analysis was carried out using an ESI-Quad 1100(A) Series MSD LC-MS system (Agilent) equipped with a Synergi Polar-RP 80 250 × 2.0 mm column (Phenomenex). Preparative RP-HPLC was performed using a Nucleodur C_{18} (ec) 250 × 21 mm column combined with an Agilent 1100 HPLC system. Protein purification was carried out using an Äkta Prime system (GE Healthcare Life Sciences). Radioactivity measurements were performed using a Packard Tricarb 2100TR liquid scintillation analyzer.

Isolation and Structure Elucidation of Mirubactin (1). *A. mirum* was grown for 4−5 days in GYM medium (glucose 4 g/L, yeast extract 4 g/L, malt extract 10 g/L, pH 7.2) at 28 °C and 250 rpm and subsequently used to inoculate iron-depleted Hagerdahl medium[56] (1:100 v/v) in 500 mL polycarbonate flasks. The production cultures were grown for 3 days at 28 °C and 250 rpm until a CAS-positive reaction of the culture supernatant was observed. After centrifugation (30 min, 6000 rpm) the supernatant was filtered (0.2 μm) and subsequently subjected to preparative RP-HPLC. Elution was performed by applying a solvent gradient of water−0.1% TFA (solvent A) and acetonitrile−0.1% TFA (solvent B) at a flow rate of 18 mL/min: linear increase from 10% to 25% B within 35 min followed by a linear increase to 95% B in 3 min, holding B for an additional 5 min before returning to 10% B in 2 min. The wavelengths chosen for detection were 215 and 280 nm, respectively. Siderophore-containing fractions were identified by CAS assay[18] and ESIMS analysis. Positive fractions were combined, lyophilized, and stored at −20 °C until further usage.

*Mirubactin (**1**):* UV (H_2O) λ_{max} (log ε) 330 (3.41) nm; IR (KBr) ν_{max} 3306, 1740, 1665, 1587, 1540, 1488, 1461, 1278, 1200.7, 1137, 1075, 845, 800, 745, and 723 cm^{-1}; ^1H NMR and ^{13}C NMR, see Supporting Information, Table S1; HRESIMS *m*/*z* 605.2192 $[M + H]^+$ (calcd for $C_{26}H_{33}N_6O_{11}^+$, 605.2202).

*holo-Mirubactin (**2**):* UV (H2O) λ_{max} (log ε) 330 (3.59), 510 (3.33) nm; HRESIMS *m*/*z* 656.1176 $[M]^-$ (calcd for $C_{26}H_{28}FeN_6O_{11}^-$, 656.1176).

Determination of Amino Acid Stereoconfiguration. To determine the absolute stereoconfiguration of the mirubactin building blocks, total hydrolysis was coupled with a derivatization method using *N*-α-(2,4-dinitro-5-fluorophenyl)-L-alaninamide (FDAA, Marfey's reagent).[24]

Five hundred micrograms of purified mirubactin was hydrolyzed by the addition of 400 μL of 6 M HCl and incubation at 95 °C for 24 h. The lyophilized hydrolysate was resuspended in 10 μL of 1 M $NaHCO_3$. A 1% solution of FDAA in acetone was added (170 μL) followed by an incubation at 37 °C for 1 h. The derivatization reaction was terminated by the addition of 20 μL of 1 M HCl. FDAA derivatives of amino acid standards (L/D-Arg, L-Orn) were prepared by incubation of 25 μL of 50 mM amino acid solution with 50 μL of 1% FDAA solution and 10 μL of 1 M $NaHCO_3$ at 37 °C for 1 h. After lyophilization, the products were resuspended in 200 μL of a 1:1 water−0.1% TFA:acetonitrile−0.1% TFA solution and analyzed by

RP-LCMS utilizing the following gradient: 0−30 min, 0−30% buffer A (10 mM ammonium formate, 1% methanol, 5% acetonitrile, pH 5.2) into buffer B (10 mM ammonium formate, 1% methanol, 60% acetonitrile, pH 5.2) followed by a linear increase to 95% B in 2 min and holding 95% B for an additional 5 min. For detection a wavelength of 340 nm was used as well as single ion monitoring, the column temperature was set to 25 °C, and a flow rate of 0.3 mL/min was employed.

Cloning, Expression, and Purification of MrbC, MrbJ-A1, and MrbJ-A2. The genes coding for MrbC, MrbJ-A1, and MrbJ-A2 were amplified by polymerase chain reaction (PCR) from genomic DNA, extracted from *A. mirum*, using the Phusion High-Fidelity DNA Polymerase with GC buffer according to the manufacturer's protocol. For the construction of the excised A-domain constructs a secondary structure prediction of the MrbJ protein was carried out using PSIPRED.[57] The excision sites were chosen in a way that the resulting A-domains contained all 10 core motifs, and no secondary structure elements (α-helices and β-strands) were disrupted. The purified and digested PCR products (MrbC: NcoI, XhoI; MrbJ-A1/A2: NcoI, NotI) were ligated into the pET28a expression vector, and the constructs confirmed by DNA sequencing. After transformation of Rosetta 2 (DE3) pLysS cells, expression and purification of the three proteins followed the same general protocol and are detailed as follows. The transformed cells were grown at 25 °C to an OD_{600} of 0.5 in LB medium. Then the cultures were induced using isopropyl-β-D-thiogalactopyranoside (final concentration 0.05 mM) and grown for an additional 3 h at 25 °C. The cells were harvested by centrifugation (7000 rpm, 20 min, 4 °C), resuspended in buffer A (50 mM HEPES, 100 mM NaCl, 20 mM imidazole, pH 8.0), and lysed by French press (SLM Aminco, Thermo French press). Cell debris was removed by centrifugation (17 000 rpm, 40 min, 4 °C), and Ni-NTA affinity chromatography was performed. The Ni-NTA column was equilibrated with buffer A, and after applying the sample, bound protein was eluted by employing gradient elution with increasing imidazole concentration (2−95% B in 30 min; buffer B contained 50 mM HEPES, 100 mM NaCl, and 200 mM imidazole, pH 8.0). Designated protein fractions were identified by SDS-PAGE, combined, concentrated, and subjected to buffer exchange (25 mM HEPES, 50 mM NaCl, pH 7.0) using a HiPrep desalting column (GE Healthcare Life Sciences). Obtained proteins were flash-frozen in liquid nitrogen and stored at −80 °C until further usage.

ATP-[^{32}P]-PP_i Exchange Assay. A typical assay contained, in a total volume of 500 μL, 5 mM substrate, 1 mM ATP, 10 mM $MgCl_2$, 5 mM $NaPP_i$, and 2 μM enzyme (MrbC, MrbJ-A1, or MrbJ-A2). Before starting the reaction by the addition of the respective enzyme, 50 μL of Na[^{32}P]PP_i solution (~2.0 × 10^7 cpm/mL) was added. The reaction was incubated at 30 °C for 30 min and subsequently quenched with 750 μL of charcoal suspension (100 mM $NaPP_i$, 600 mM $HClO_4$, 1.6% (w/v) charcoal). After two washing steps using wash solution (100 mM $NaPP_i$, 600 mM $HClO_4$) the resuspended charcoal was transferred into 4 mL of scintillation solution (Rotiszint, Carl Roth), and radioactivity measurements were carried out. All reactions were performed in triplicate

■ ASSOCIATED CONTENT

Supporting Information

MS^2 and MS^3 fragmentation spectra, table of chemical shifts and NMR spectra, IR spectrum of mirubactin, LCMS of *apo*- and *holo*-mirubactin, UV/vis spectra of *apo*- and *holo*-mirubactin, determination of amino acid stereochemistry, foroxymicin/erythrochelin-like cluster in *A. mirum*, *mrb*-gene cluster comparison, bioinformatic overview of *mrb*-gene cluster, SDS-PAGE gels of MrbJ-A1, MrbJ-A2, and MrbC, complete refs 16 and 17. This material is available free of charge via the Internet at http://pubs.acs.org.

■ AUTHOR INFORMATION

Corresponding Author

*Tel: +49 (0) 6421 28 25722. Fax: +49 (0) 6421 28 22191. E-mail: marahiel@staff.uni-marburg.de.

Notes

The authors declare no competing financial interest.

■ ACKNOWLEDGMENTS

We gratefully acknowledge the Deutsche Forschungsgemeinschaft (DFG) and the LOEWE Center for Synthetic Microbiology (SYNMIKRO) for financial support.

■ REFERENCES

(1) Hider, R. C.; Kong, X. *Nat. Prod. Rep.* **2010**, *27*, 637−657.
(2) Winkelmann, G.; Drechsel, H. *Microbial Siderophores*; Wiley-VCH: Weinheim, 1997.
(3) Peuckert, F.; Miethke, M.; Albrecht, A. G.; Essen, L. O.; Marahiel, M. A. *Angew. Chem., Int. Ed.* **2009**, *48*, 7924−7927.
(4) Miethke, M.; Klotz, O.; Linne, U.; May, J. J.; Beckering, C. L.; Marahiel, M. A. *Mol. Microbiol.* **2006**, *61*, 1413−1427.
(5) Andrews, S. C.; Robinson, A. K.; Rodriguez-Quinones, F. *FEMS Microbiol. Rev.* **2003**, *27*, 215−237.
(6) Challis, G. L. *ChemBioChem* **2005**, *6*, 601−611.
(7) Miethke, M.; Marahiel, M. A. *Microbiol. Mol. Biol. Rev.* **2007**, *71*, 413−451.
(8) Seyedsayamdost, M. R.; Traxler, M. F.; Zheng, S. L.; Kolter, R.; Clardy, J. *J. Am. Chem. Soc.* **2011**, *133*, 11434−11437.
(9) Bosello, M.; Robbel, L.; Linne, U.; Xie, X.; Marahiel, M. A. *J. Am. Chem. Soc.* **2011**, *133*, 4587−4595.
(10) Dimise, E. J.; Widboom, P. F.; Bruner, S. D. *Proc. Natl. Acad. Sci. U. S. A.* **2008**, *105*, 15311−15316.
(11) Lautru, S.; Deeth, R. J.; Bailey, L. M.; Challis, G. L. *Nat. Chem. Biol.* **2005**, *1*, 265−269.
(12) Yu, T. W.; Bai, L.; Clade, D.; Hoffmann, D.; Toelzer, S.; Trinh, K. Q.; Xu, J.; Moss, S. J.; Leistner, E.; Floss, H. G. *Proc. Natl. Acad. Sci. U. S. A.* **2002**, *99*, 7968−7973.
(13) Murao, S.; Imafuku, S.; Oyama, H. *Biosci. Biotechnol. Biochem.* **1997**, *61*, 561−562.
(14) Ozasa, T.; Yoneda, T.; Hirasawa, M.; Suzuki, K.; Tanaka, K.; Kadota, S.; Iwanami, M. *J. Antibiot. (Tokyo)* **1991**, *44*, 768−773.
(15) Watanabe, K.; Okuda, T.; Yokose, K.; Furumai, T.; Maruyama, H. B. *J. Antibiot. (Tokyo)* **1983**, *36*, 321−324.
(16) Land, M.; Lapidus, A.; Mayilraj, S.; Chen, F.; Copeland, A.; Del Rio, T. G.; Nolan, M.; Lucas, S.; Tice, H.; Cheng, J. F.; Chertkov, O.; Bruce, D.; Goodwin, L.; Pitluck, S.; Rohde, M.; Goker, M.; Pati, A.; Ivanova, N.; Mavromatis, K.; Chen, A.; Palaniappan, K.; Hauser, L.; Chang, Y. J.; Jeffries, C. C.; Brettin, T.; Detter, J. C.; Han, C.; Chain, P.; Tindall, B. J.; Bristow, J.; Eisen, J. A.; Markowitz, V.; Hugenholtz, P.; Kyrpides, N. C.; Klenk, H. P. *Stand. Genomic Sci.* **2009**, *1*, 46−53.
(17) Parish, C. A.; Smith, S. K.; Calati, K.; Zink, D.; Wilson, K.; Roemer, T.; Jiang, B.; Xu, D.; Bills, G.; Platas, G.; Pelaez, F.; Diez, M. T.; Tsou, N.; McKeown, A. E.; Ball, R. G.; Powles, M. A.; Yeung, L.; Liberator, P.; Harris, G. *J. Am. Chem. Soc.* **2008**, *130*, 7060−7066.
(18) Schwyn, B.; Neilands, J. B. *Anal. Biochem.* **1987**, *160*, 47−56.
(19) de Carvalho, P. S.; Nachtigall, F. M.; Eberlin, M. N.; Moraes, L. A. *J. Org. Chem.* **2007**, *72*, 5986−5993.
(20) Lazos, O.; Tosin, M.; Slusarczyk, A. L.; Boakes, S.; Cortes, J.; Sidebottom, P. J.; Leadlay, P. F. *Chem. Biol.* **2010**, *17*, 160−173.
(21) Tappe, R.; Taraz, K.; Budzikiewicz, H.; Meyer, J. M.; Lefevre, J. F. *J. Prak. Chem.-Chem. Ztg.* **1993**, *335*, 83−87.
(22) Sever, M. J.; Wilker, J. J. *Dalton Trans.* **2004**, 1061−1072.
(23) Jalal, M. A.; Helm, D. V. *Isolation and Spectroscopic Identification of Fungal Siderophores*; CRC Press: Boca Raton, 1991.
(24) Bhushan, R.; Bruckner, H. *Amino Acids* **2004**, *27*, 231−247.
(25) Crumbliss, A. L.; Harrington, J. M. *Iron Sequestration by Small Molecules: Thermodynamic an Kinetic Studies of Natural Siderophores and Synthetic Model Compounds*; Academic Press: New York, 2009.

(26) Ghosh, A.; Ghosh, M.; Niu, C.; Malouin, F.; Moellmann, U.; Miller, M. J. *Chem. Biol.* **1996**, *3*, 1011−1019.
(27) Schobert, R.; Stangl, A.; Hannernann, K. *Tetrahedron* **2008**, *64*, 1711−1720.
(28) Biggins, J. B.; Gleber, C. D.; Brady, S. F. *Org. Lett.* **2011**, *13*, 1536−1539.
(29) Challis, G. L. *J. Med. Chem.* **2008**, *51*, 2618−2628.
(30) Robbel, L.; Knappe, T. A.; Linne, U.; Xie, X.; Marahiel, M. A. *FEBS J.* **2010**, *277*, 663−676.
(31) Umezawa, H.; Aoyagi, T.; Ogawa, K.; Obata, T.; Iinuma, H.; Naganawa, H.; Hamada, M.; Takeuchi, T. *J. Antibiot. (Tokyo)* **1985**, *38*, 1813−1815.
(32) Chen, Y.; Ntai, I.; Ju, K. S.; Unger, M.; Zamdborg, L.; Robinson, S. J.; Doroghazi, J. R.; Metcalf, W. W.; Kelleher, N. L. *J. Proteome Res.* **2012**, *11*, 85−94.
(33) Fischbach, M. A.; Walsh, C. T. *Chem. Rev.* **2006**, *106*, 3468−3496.
(34) Schwecke, T.; Aparicio, J. F.; Molár, I.; König, A.; Khaw, L. E.; Haydock, S. F.; Oliynyk, M.; Caffrey, P.; Cortés, J.; Lester, J. B.; Böhm, G. A.; Staunton, J.; Leadlay, P. F. *Proc. Natl. Acad. Sci. U. S. A.* **1995**, *92*, 7839−7843.
(35) Motamedi, H.; Shafiee, A. *Eur. J. Biochem.* **1998**, *256*, 528−534.
(36) Walsh, C. T.; Haynes, S. W.; Ames, B. D.; Gao, X.; Tang, Y. *Biochemistry* **2011**, *50*, 5668−5679.
(37) von Dohren, H. *Fungal Genet. Biol.* **2009**, *46*, 45−52.
(38) Patzer, S. I.; Braun, V. *J. Bacteriol.* **2010**, *192*, 426−435.
(39) Gehring, A. M.; Mori, I.; Walsh, C. T. *Biochemistry* **1998**, *37*, 2648−2659.
(40) Walsh, C. T.; Liu, J.; Rusnak, F.; Sakaitani, M. *Chem. Rev.* **1990**, *90*, 1105−1129.
(41) Rottig, M.; Medema, M. H.; Blin, K.; Weber, T.; Rausch, C.; Kohlbacher, O. *Nucleic Acids Res.* **2011**, *39*, W362−W367.
(42) May, J. J.; Kessler, N.; Marahiel, M. A.; Stubbs, M. T. *Proc. Natl. Acad. Sci. U. S. A.* **2002**, *99*, 12120−12125.
(43) Rowland, B. M.; Grossman, T. H.; Osburne, M. S.; Taber, H. W. *Gene* **1996**, *178*, 119−123.
(44) Sutcliffe, I. C.; Russell, R. R. *J. Bacteriol.* **1995**, *177*, 1123−1128.
(45) Wang, S.; Wu, Y.; Outten, F. W. *J. Bacteriol.* **2011**, *193*, 563−574.
(46) Butterton, J. R.; Calderwood, S. B. *J. Bacteriol.* **1994**, *176*, 5631−5638.
(47) Robbel, L.; Helmetag, V.; Knappe, T. A.; Marahiel, M. A. *Biochemistry* **2011**, *50*, 6073−6080.
(48) Bosello, M.; Mielcarek, A.; Giessen, T. W.; Marahiel, M. A. *Biochemistry* **2012**, *51*, 3059−3066.
(49) Breazeale, S. D.; Ribeiro, A. A.; McClerren, A. L.; Raetz, C. R. *J. Biol. Chem.* **2005**, *280*, 14154−14167.
(50) Medema, M. H.; Blin, K.; Cimermancic, P.; de Jager, V.; Zakrzewski, P.; Fischbach, M. A.; Weber, T.; Takano, E.; Breitling, R. *Nucleic Acids Res.* **2011**, *39*, W339−W348.
(51) Miller, M. J.; Lin, Y. M. *J. Org. Chem.* **1999**, *64*, 7451−7458.
(52) Walsh, C. T.; Chen, H.; Keating, T. A.; Hubbard, B. K.; Losey, H. C.; Luo, L.; Marshall, C. G.; Miller, D. A.; Patel, H. M. *Curr. Opin. Chem. Biol.* **2001**, *5*, 525−534.
(53) Zaleta-Rivera, K.; Xu, C.; Yu, F.; Butchko, R. A.; Proctor, R. H.; Hidalgo-Lara, M. E.; Raza, A.; Dussault, P. H.; Du, L. *Biochemistry* **2006**, *45*, 2561−2569.
(54) Lin, S.; Van Lanen, S. G.; Shen, B. *Proc. Natl. Acad. Sci. U. S. A.* **2009**, *106*, 4183−4188.
(55) Berger, S.; Braun, S. *200 and More NMR Experiments, a Practical Course*; Wiley-VCH: Weinheim, 2004.
(56) Hagerdal, B.; Ferchak, J. D.; Pye, E. K. *Biotechnol. Bioeng.* **1980**, *22*, 1515−1526.
(57) Jones, D. T. *J. Mol. Biol.* **1999**, *292*, 195−202.